Plastic vortex creep and dimensional crossovers in the highly anisotropic superconductor $HgBa_2CuO_{4+x}$

Haley M. Cole [1], Michael B. Venuti [1], Brian Gorman [2], Eric D. Bauer [3], Mun K. Chan [4] and Serena Eley [1,5,*]

[1] *Department of Physics, Colorado School of Mines, Golden, Colorado 80401, USA*

[2] *Department of Materials and Metallurgical Engineering, Colorado School of Mines, Golden, Colorado 80401, USA*

[3] *Los Alamos National Laboratory, Los Alamos, New Mexico 87545, USA*

[4] *Pulsed Field Facility, National High Magnetic Field Laboratory, Los Alamos National Laboratory, Los Alamos, New Mexico 87545, USA*

[5] *Department of Electrical & Computer Engineering, University of Washington, Seattle, Washington 98155, USA*

(Received 22 December 2021; revised 31 January 2023; accepted 16 February 2023; published 14 March 2023)

In type-II superconductors exposed to magnetic fields between upper and lower critical values, H_{c1} and H_{c2}, penetrating magnetic flux forms a lattice of vortices whose motion can induce dissipation. Consequently, the magnetization M of superconductors is typically progressively weakened with increasing magnetic field $B \propto n_v$ (for vortex density n_v). However, some materials exhibit a nonmonotonic $M(B)$, presenting a maximum in M at what is known as the second magnetization peak. This phenomenon appears in most classes of superconductors, including low-T_c materials, iron-based, and cuprates, complicating pinpointing its origin and garnering intense interest. Here we report on vortex dynamics in optimally doped and overdoped $HgBa_2CuO_{4+x}$ crystals, with a focus on a regime in which plastic deformations of the vortex lattice govern magnetic properties. Specifically, we find that both crystals exhibit conspicuous second magnetization peaks and, from measurements of the field- and temperature-dependent vortex creep rates, identify and characterize phase boundaries between elastic and plastic vortex dynamics, as well as multiple previously unreported transitions within the plastic flow regime. We find that the second magnetization peak coincides with the elastic-to-plastic crossover for a very small range of high fields and a sharp crossover within the plastic flow regime for a wider range of lower fields. Moreover, we find evidence that this transition in the plastic flow regime is due to a dimensional crossover, specifically, a transition from three to two-dimensional plastic dynamics.

DOI: 10.1103/PhysRevB.107.104509

I. INTRODUCTION

The electromagnetic properties of many seemingly disparate condensed-matter systems are dictated by the dynamics of inlying elastic media—including charge density waves in materials with highly anisotropic band structure [1], domain walls in ferroelectrics, skyrmions in magnets with strong spin-orbit coupling [2], and vortex matter in type-II superconductors [3]. In these systems, competition between disorder, elasticity, thermal energy, and driving forces from currents can engender elastic or plastic deformations and determine phase boundaries between the two regimes. In superconductors, plastic flow has received considerably less attention than elastic and glassy regimes, despite its technological relevance for, e.g., large-scale high-T_c applications that tend to operate at high temperatures ($T/T_c > 0.5$) and fields, often within the plastic flow regime.

A lattice of vortices forms in type-II superconductors exposed to magnetic fields in between the lower and upper critical fields, H_{c1} and $H_{c2} = \Phi_0/2\pi\mu\xi_{ab}^2$, respectively. These vortices are nanoscale regions of penetrating magnetic flux, each carrying a single flux quantum Φ_0. Consequently, the vortex core is nonsuperconducting, of diameter $2\xi_{ab}(T)$, and surrounded by circulating supercurrents which decay within a characteristic length $\lambda_{ab}(T)$. Here, ξ_{ab} is the in-plane coherence length, λ_{ab} is the in-plane penetration depth, and T is the temperature.

Propelled by current-induced forces and thermal energy, vortex motion is a major source of dissipation in superconductors. Counteracting these forces, vortices are immobilized by material defects that collectively define the vortex pinning potential. Vortices are elastic objects that can accommodate to the pinning potential by elastic deformation, bending to find the most energetically favorable shape and position within this potential. This deformation costs an elastic energy $U_{el} \sim \varepsilon_l(\xi_{ab}/L)^2 L$, for $\varepsilon_l = \varepsilon_0 = (\Phi_0/4\pi\lambda_{ab})^2$ is the vortex line tension, and L is the vortex segment length [4]. Ultimately, competition between the thermal energy, current-induced forces, pinning forces, vortex elasticity, and vortex-vortex interactions determines the nature of vortex dynamics, e.g., whether it is elastic or plastic.

In the elastic regime, vortices may elastically deform while remaining in their equilibrium positions in a quasiordered phase, and the system starts to melt when thermal energy surpasses the elastic energy barriers. The energy barrier that pins vortices, $U(J) \propto J^{-\mu}$, grows infinitely with decreasing current density J (signifying a glass state), characterized by the glassy exponent $\mu > 0$ [4]. When $U(J)$ surpasses the plastic energy barrier, plastic flow occurs, which qualitatively differs from the elastic regime in that there are different vortex channels with different dynamics.

*serename@uw.edu

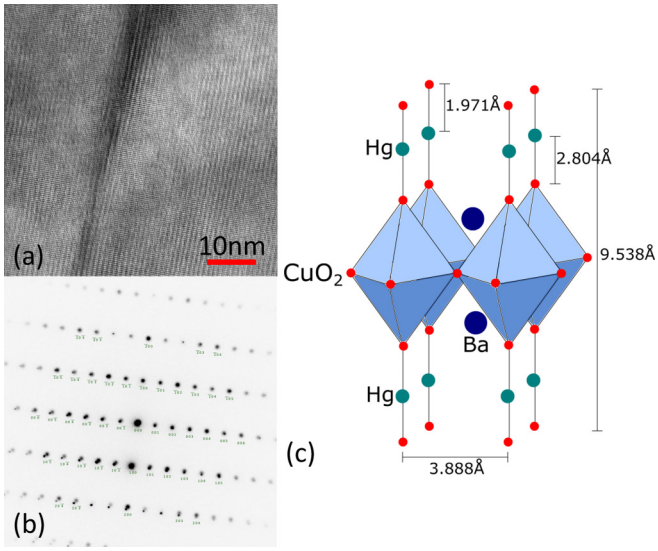

FIG. 1. (a) High-resolution bright field transmission electron micrograph of a planar defect in an optimally doped Hg1201 single crystal. (b) Selected area electron diffraction pattern overlaid with a simulated pattern using a [001] zone axis. The planar defect is observed to exist on the (100) plane of the tetragonal structure shown in (c). (c) Crystal structure of Hg1201, featuring tetragonal symmetry in the space group $P4/mmm$ and a single CuO_2 plane per primitive cell [44].

In the plastic flow regime, coherent domains of the vortex lattice are separated by dislocations (line defects) and motion can be dislocation mediated, similar to the diffusion of dislocations in atomic solids [5,6]. Some domains may be static, whereas others may move at different rates relative to each other [7,8]. These dynamics are often likened to that of conglomerates of ice floes, in which each ice floe is analogous to a quasiordered domain of vortices. Vortex motion may then occur through a variety of distinct dynamic arrangements. For example, channels of moving vortices can flow between stationary vortex lattice islands [9–11], or large quasiordered domains (ice floe) can slide with respect to each other [6].

One way to determine the relevant energy barriers and ultimately assess whether the dynamics are elastic or plastic is to study the rate of thermal activation over these barriers—the vortex creep rate. Collective creep theory predicts that, in the elastic regime, $U_{el}(B, J) = U_0(B)(J_c/J)^{\mu} \propto B^{\nu}J^{-\mu}$ for magnetic field B, critical current density J_c, and positive critical exponents ν and μ, whereas in the plastic flow regime the energy barrier U_{pl} is nondiverging with increasing J [4,6,12]. The creep process is determined by the lowest of the two energy barriers: consequently, a crossover to the plastic flow regime is expected when U_{pl} becomes less than U_{el}, generally at low J or high B.

A common, conspicuous signature of a crossover between vortex pinning regimes is the appearance of a peak in the magnetization $M(H)$ at intermediate fields, known as the second magnetization peak (SMP). This peak is intriguing because $M \propto J_c$, and J_c typically decreases monotonically with increasing field (vortex density). Remarkably, such nonmonotonic behavior indicates an improvement in J_c with increasing density of dissipatively moving vortices. Second magnetization peaks have been reported in studies of most classes of superconductors, including low-T_c [13,14], iron-based [15–25], highly anisotropic [26,27] materials and other cuprates [21,28–31], as well as previous work on Hg1201 [32–37]. This peak is typically thought to originate from elastic-to-plastic transitions [15,17,18,20], structural phase transitions [38–41] in the vortex lattice, or dimensional crossovers.

Here we report on a systematic study of vortex dynamics in $HgBa_2CuO_{4+x}$ (Hg1201) single crystals, ideal testbeds for studying the effects of thermal fluctuations on three- and two-dimensional (3D, 2D) vortex dynamics as well as dimensional crossovers, owing to high anisotropy and high critical temperature T_c. Hg1201 is also of broad interest due to the presence of charge-density-wave correlations that cause quantum oscillations at low temperatures [42,43]. Using extensive magnetization studies, we map the appearance of a second magnetization peak at $H_{\rm smp}(T)$, a crossover between elastic and plastic dynamics at $H_{ep}(T)$, and crossovers within the plastic flow regime suggesting multiple distinct dynamic arrangements. Notably, we find that the second magnetization peak coincides with the elastic-to-plastic crossover at high magnetic fields and low temperatures and a crossover within the plastic flow regime at intermediate fields and temperatures. It may also correspond with a dimensional crossover from 3D to 2D plastic dynamics.

II. RESULTS AND DISCUSSION

We grew, analyzed the microstructure of, and performed magnetization studies on an optimally doped and an overdoped Hg1201 single crystal. Details on the growth method are provided in the Methods section. Transmission electron microscopy studies of the optimally doped crystal, shown in Fig. 1, reveal a clean microstructure, with only dislocations evident within the resolution of our system. Accordingly, our crystals are absent of defects that could exert strong pinning forces on vortices (such as twin boundaries or large precipitates), such that we may expect vortex pinning to primarily originate from weak collective effects from point disorder and that the effects of anisotropy may strongly influence magnetic properties.

Magnetization measurements $M(T, H, t)$ were performed using a Quantum Design superconducting quantum interference device (SQUID) magnetometer in which the magnetic field was aligned with the sample's c axis ($H \parallel c$), T indicates temperature, and t is time. The magnetization results from the magnetic moments of circulating currents in the sample, including the currents around vortex flux lines and the Meissner currents that circulate at the surface of the sample. By measuring M versus T at 5 Oe, after zero-field cooling, we find that the onset critical temperatures T_c of the optimally and overdoped crystals are 95.9 K and 90.0 K, respectively, as shown in Fig. 2, and is consistent with previous work [34,45–48]. Moreover, in both samples the transition width is narrow, suggestive that the sample is high quality and homogeneous.

Figure 3 shows the isothermal field-dependent magnetization $M(H)$ curves collected for both samples. The curves exhibit a SMP at $H_{\rm smp}$. In a previous study [32] of an optimally doped Hg1201 crystal, we found that the elastic-to-plastic crossover is not responsible for the SMP in Hg1201.

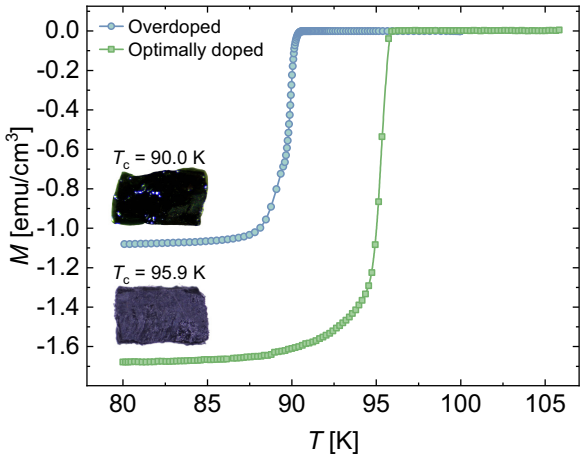

FIG. 2. Temperature-dependent magnetization $M(T)$ measured at $\mu_0 H = 5$ Oe after zero-field cooling, revealing $T_c = 95.9$ K and $T_c = 90.0$ K, for our optimally doped and overdoped samples, respectively. The insets display optical images of the samples.

Though we did note a correspondence between the SMP and the elastic-to-plastic crossover at low temperatures $T/T_c < 0.2$, this overlap disappears at higher temperatures, in which the SMP occurred within the plastic flow regime. In this work we compare the field and temperature at which the second magnetization peak occurs to the elastic-to-plastic crossover and then proceed to characterize the plastic flow regime, which shows evidence of distinct dynamics arrangements that may be responsible for the SMP. To this end we extract the elastic and plastic energy barriers, and their dependencies on the current and magnetic field, from magnetic relaxation measurements to determine the vortex creep rates.

Vortex creep measurements allow us to probe the vortex structure, dynamics, and interactions (e.g., vortex-vortex, vortex-defect). The vortex creep rate naturally depends on the energy barrier that must be overcome for vortex motion. According to collective creep theories, this energy barrier,

$$U_{\rm act}(J) = (U_p/\mu)[(J_{c0}/J)^{\mu} - 1], \tag{1}$$

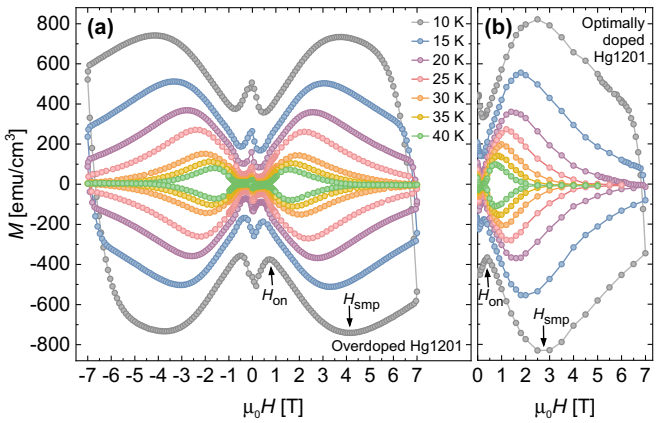

FIG. 3. Isothermal magnetic hysteresis loops $M(H)$ at select temperatures for our (a) overdoped and (b) optimally doped Hg1201 single crystals. Each curve exhibits a second magnetization peak at $H_{\rm smp}$ and low-field dip at H_{on}.

depends on the critical current in the absence of thermal activation J_{c0}, energy barrier U_p (at $J = 0$), and the glassy exponent μ, which is related to the size and dimensionality of the vortex bundle that hops during the creep process [4,49]. Specifically, μ depends on whether dynamics are driven by single vortices or a vortex bundle of lateral dimension R_c smaller than (small bundle), comparable to (medium bundle), or larger than (large bundle) the penetration depth λ_{ab}. For example, for 3D vortices, the dynamics of single vortices, small vortex bundles, and large vortex bundles are expected to produce a μ of 1/7, 3/2 or 5/2, and 7/9, respectively [4]. In the case of 2D vortices, $\mu = 7/4$, 13/16, and 1/2 is expected for creep of small, medium, and large vortex bundles, respectively [4,50,51].

By combining Eq. (1) with the creep time $t = t_0 e^{U_{\rm act}(J)/k_B T}$ (related to the vortex penetration time [49]), we find that the dissipation generated by creep should cause the persistent current to decay over time as $J(t) = J_{c0}[1 + (\mu k_B T/U_p)\ln(t/t_0)]^{-1/\mu}$ and that the thermal vortex creep rate is

$$S \sim \left|\frac{d\ln J}{d\ln t}\right| = \frac{k_B T}{U_p + \mu k_B T \ln(t/t_0)}, \tag{2}$$

where $t_0 \approx 1 - 10$ μs [49].

Because the magnetization in type-II superconductors is proportional to current ($M \propto J$), creep rates can readily be extracted from measurements of M versus time t. Likewise, as seen from Eq. (2), knowledge of $S(T, H)$ provides access to both U_p and μ. Consequently, creep measurements are indispensable for revealing the size of the energy barrier, determining its dependence on current, field, and temperature, and also ascertaining whether the dynamics are particlelike, elastic, or plastic.

Figure 4(a) shows the temperature and field dependence of the creep rates in both Hg1201 crystals. The raw data showing $M(t)$, from which S was extracted, is presented in the Supplemental Material [52]. Over most of the temperature and field range, the creep rate increases monotonically with temperature and field, with a few exceptions. First, in both samples creep at the lowest fields is faster than at higher fields and temperature independent between 1.8 and 40 K, plateauing at around $S \sim 0.06$. Second, data for the overdoped sample exhibits a small, anomalous peak in $S(T)$ at around 45 K to 48 K for fields of 1.25 T to 2.1 T. Lastly, in both samples S decreases with increasing temperature up to 25–30 K then positively correlates with further increases in temperature. These different dynamics at low fields may be related to the mechanism responsible for the low-field dip at H_{on} (Fig. 3), which is unresolved in many materials. In Ref. [32] we found a dip in $S(H)$ near H_{on}, which was later shown in Ref. [25] to be a common trend among many materials, including some other highly anisotropic materials (e.g., $Bi_2Sr_2CaCu_2O_{8+x}$), some less anisotropic cuprates (e.g., $YBa_2Cu_3O_{7-x}$), iron-based superconductors (e.g., $BaFe_2(As_{0.72}P_{0.28})_2$), and (K, Ba)$BiO_3$ [25].

The low-field plateau in $S(T)$ is a signature of glassiness over a broad temperature range, as seen in $YBa_2Cu_3O_{7-x}$ single crystals [53]. From Eq. (2) we may expect a plateau to occur when $U_p \ll \mu_0 k_B T \ln(t/t_0)$ such that $S \sim [\mu \ln(t/t_0)]^{-1}$ becomes independent of temperature. For our measurement

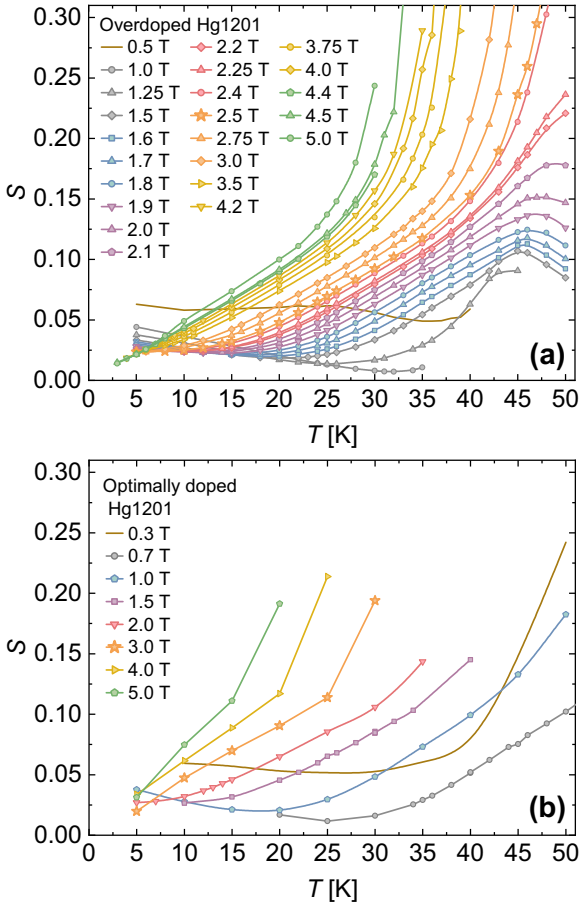

FIG. 4. Temperature dependence of the vortex creep rates in different applied magnetic fields for (a) the overdoped and (b) the optimally doped Hg1201 crystals. The error bars are determined from the standard deviations of linear fit to $\log m - \log t$ (where m is the magnetic moment) and are smaller than the symbol size.

window of $t \sim 1$ hour, $\ln(t/t_0) \approx 27$ such that $\mu \sim 0.6$, close to the expectation of 0.5 for creep of large bundles of 2D vortices in both samples [4,50,51].

A. Elastic vortex dynamics and the elastic-to-plastic crossover

Analysis of the current dependence of the effective activation energy can provide direct experimental access to μ, given that U_p is typically otherwise unknown. Combining Eqs. (1) and (2), and considering the exponential for the creep time t_0, we find that the effective pinning energy is

$$U^\star \equiv \frac{T}{S} = U_p\left(\frac{J_{c0}}{J}\right)^{\mu}. \tag{3}$$

Accordingly, as we see from Eq. (3), the exponent can easily be extracted from the slopes of $U^\star$ vs $1/J$ on a log-log plot. Figure 5 shows $U^\star(1/J)$ collected at multiple fields for both crystals. Notice that the curves are approximately linear within distinct regimes and exhibit the prominent change from positive to negative slope that is associated with an elastic-to-plastic crossover at $H_{ep}(T)$.

First focusing on the elastic dynamics in the overdoped crystal, Fig. 5(c) displays the field dependence of the glassy

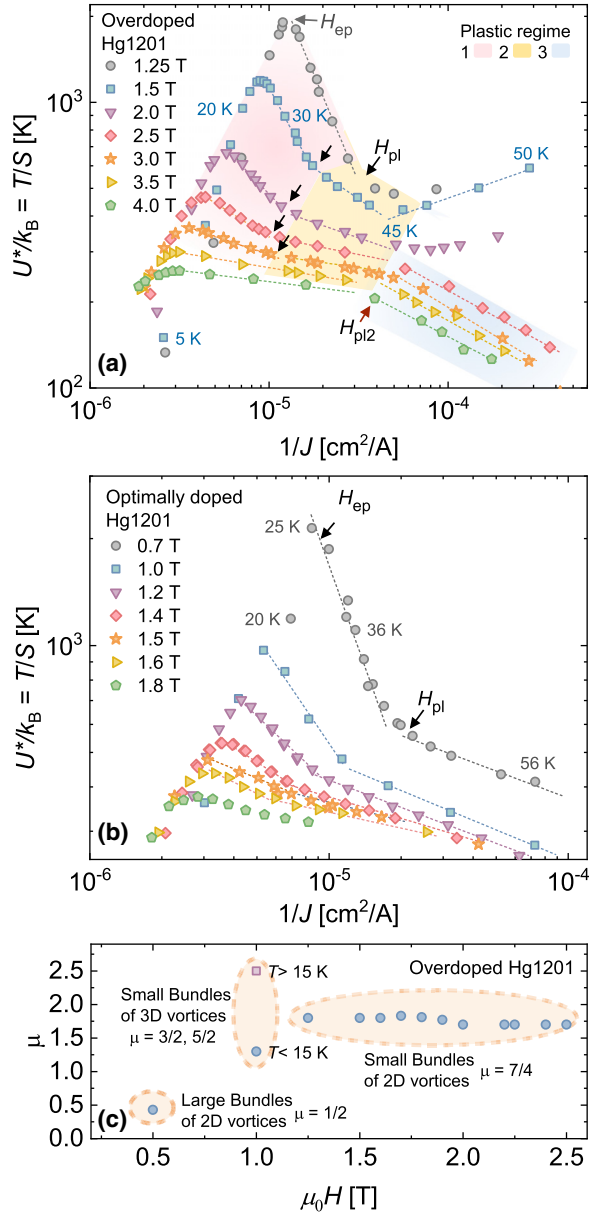

FIG. 5. (a) Energy scale U^* plotted against $1/J$ for the overdoped Hg1201 crystal measured in applied magnetic fields 1.25 to 4 T. Data was collected at 0.2-T intervals; for clarity, only select curves are displayed. Temperatures at which data was collected are noted for select data points; at fixed field, temperature increases with $1/J$. Dashed lines are examples of linear fits used to extract glassy and plastic exponents, noted in Fig. 8 and the main text. Change from a positive to negative slope suggests a crossover from elastic-to-plastic vortex dynamics at H_{ep}. Data collected at fields below 3.2 T exhibit two kinks in the plastic flow regime at H_{pl} (lowest T kink, identified with black arrows) and H_{pl2}. Higher fields display only one kink, at H_{pl2} (example labeled with red arrow). Plastic flow regimes 1 ($H_{ep} < H < H_{pl}$), 2 ($H_{pl1} < H < H_{pl2}$), and 3 ($H > H_{pl2}$) identified by red, yellow, and blue shading, respectively. (b) U^* vs $1/J$ for the optimally doped Hg1201 crystal. (c) Field dependence of the glassy exponent in the overdoped sample. Labels indicate theoretical expectations that most closely match experimental values.

exponent μ extracted from linear fits to the elastic regime. From the 0.5 T data, we extract $\mu \approx 0.5$, which matches the

expectation for collective creep of large bundles of 2D pancake vortices. The presence of large bundles in small fields is suggestive of a clean pinning landscape in which long-range $1/r$ vortex-vortex interactions are only weakly perturbed by vortex-defect interactions. When the field is increased to 1 T, μ becomes 1.3 at low temperatures $T < 15$ K and 2.6 at higher temperatures, close to the expectations of 3/2 and 5/2 for creep of small bundles of 3D vortices [51]. At even higher magnetic fields of 1–2.5 T, we find that $\mu \approx 1.7$–1.8, close to the expectation of 7/4 for creep of small bundles of 2D vortices.

This change from 2D to 3D to 2D dynamics with increasing field (at low fields) is consistent with predictions from numerical simulations of magnetically interacting vortices in highly anisotropic superconductors, considering long-range nonlinear interactions along the c axis [54]. Specifically, Ref. [54] found that, at very low fields, vortices are disordered within the planes, uncorrelated in the z directions, and interact strongly with pinning centers, resulting in relatively high J_c. As the field is increased, a 3D vortex lattice forms as vortices between planes align, painting a picture of 3D vortex lines that are weakly coupled to an energy landscape of point defects: the lattice stiffness increases, weakening the effectiveness of pinning and effectuating a decrease in J_c. The simulations further predict that at intermediate applied magnetic fields, pancake vortices between planes start to decouple, enabling higher effective pinning therefore higher J_c. Consequently, the 2D-3D-2D transition leads to a dip in J_c such that the simulations are not only consistent with our extracted glassy exponent, but also with the dip in $M(H) \propto J_c(H)$ at H_{on} present in the magnetization loops in Fig. 3.

Notice that the data suggests that large bundles exist at 0.5 T, whereas small bundles exist at higher fields >1.25 T. In many systems, the bundle size increases with increasing field [4]. However, this behavior is consistent with our suggestion in Ref. [32] that as H increases, the strength of pinning suddenly increases around H_{on}, causing the lattice to become more entangled and the bundle size to decrease. Consequently, we see both J_c and μ increase. Results for the optimally doped crystal are similar, as presented in the phase diagram in Fig. 8 and discussed in detail in Ref. [32].

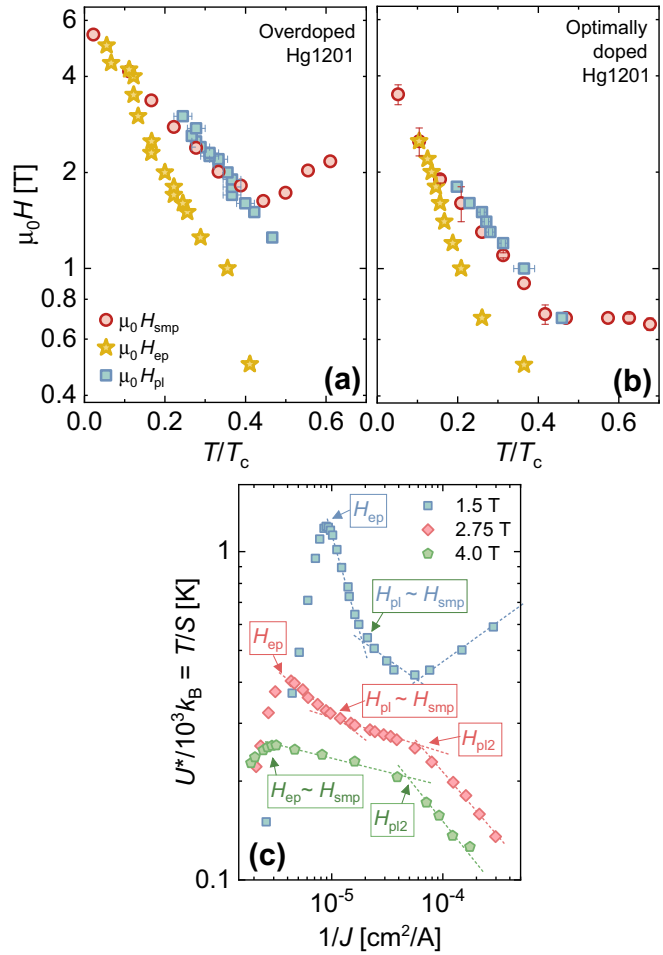

FIG. 6. Field-temperature phase diagram for (a) overdoped and (b) optimally doped Hg1201 crystals showing that the second magnetization peak coincides with the elastic-to-plastic crossover only at high fields and with the kink in the plastic flow regime (at H_{pl}) at lower fields. (c) U^* vs $1/J$ for overdoped Hg1201 crystal showing examples of three different types of behavior in plastic regime: low fields show two distinct negative slopes then an anomalous transition to a positive slope at low J; intermediate fields display three distinct negative slopes; and high fields exhibit two distinct negative slopes.

B. Plastic deformations of the vortex lattice

Collective creep theory considers elastic deformations of the vortex lattice and neglects dislocations that may govern vortex dynamics in the plastic regime. In this regime the elastic pinning barrier is sufficiently high such that plastic deformations of the vortex lattice are more energetically favorable. Abulafia *et al.* [6] first suggested that a *nondiverging* (as $J \to 0$) energy barrier $U(J)$ may be suggestive of plastic creep, compared to the *diverging* elastic barrier described in Eq. (3). Specifically, they applied an expression from dislocation theory, replaced strain with J_c, and found that the plastic activation barrier is $U_{pl}(J) = U_{pl}^0(1 - J^{1/2}/J_0)$, where J_0 is related to the plastic critical current density. They further showed that this described data collected on $YBa_2Cu_3O_{7-x}$ crystals, in a regime in which there was other evidence of plastic dynamics, such as a decrease in U with magnetic field (whereas an increase is predicted for elastic creep). Consequently, it has become common to identify a change from elastic-to-plastic creep as a sudden change in slope on a $\log U - \log(1/J)$ plot, identifying the plastic flow regime as $U_{pl} \sim (1/J)^p$, for $p < 0$, and many studies have observed a sharp change in slope with (in some cases) strikingly linear behavior on both sides of the transition [15,17,20,21,41,55–63]. At high temperatures and fields $H > H_{ep}$ in our samples, we see that the slope of the U^* versus $1/J$ plot shown in Fig. 5 becomes negative, indicative of plastic flow.

One or two kinks are clearly evident within the plastic flow regime, at the junction between linear regions with distinct slopes. For applied magnetic fields below approximately 1 T in the overdoped sample [Fig. 5(a)], we either do not observe an elastic-to-plastic transition or capture little of the plastic regime within the temperature range of our measurements. At higher magnetic fields, we observe three different trends in the $U(1/J)$ data, exemplified in Fig. 6(c). First, for fields between

1.25 and 2 T, two kinks are clearly evident within the plastic flow regime. We label the kink at the lowest temperature (lowest $1/J$) as H_{pl}; the kink that appears at a higher temperature (higher $1/J$) is followed by a transition to a positively sloped region that corresponds to the anomalous nonmonotonicity in $S(T)$ around 45 K, seen in Fig. 4(a). Second, data collected in fields between 2 and 3 T also shows two kinks defining three regions with distinct, negative slopes; we again label the lowest temperature kink as H_{pl} and also label the higher temperature one as H_{pl2}. Last, for magnetic fields higher than approximately 3 T, there appears to be only two distinct negatively sloped regions; here we label the junction as H_{pl2}.

In the following discussion we refer to the different regions as plastic regime 1 ($H_{ep} < H < H_{pl}$), regime 2 ($H_{pl} < H < H_{pl2}$), and regime 3 ($H > H_{pl2}$), identified by the red, yellow, and blue shaded regions in Fig. 5. Many questions arise from the data in Fig. 5(a). First, is one of these transitions in the plastic flow regime responsible for the second magnetization peak? What type of plastic dynamical arrangements occur in plastic regimes 1, 2, and 3? What causes the sudden increase in U^* around 46 K for the low-field data?

To answer the first question, we plot a comparison of the temperature dependence of H_{ep}, $H_{\rm smp}$, and H_{pl} in Figs. 6(a) and 6(b). The second magnetization peak $H_{\rm smp}$ coincides with H_{ep} at high fields, and we see a clear correspondence between $H_{\rm smp}$ and H_{pl} at lower fields. To our knowledge, the latter correspondence has not been previously identified. Distinguishing the dynamics in plastic regimes 1 and 2 may reveal the origin of the second magnetization peak.

Plastic deformations of the vortex lattice bend/displace vortices on a scale $u \sim a_0$, for mean intervortex separation $a_0 \sim \sqrt{\Phi_0/B}$ and flux quantum Φ_0, such that the expected field dependence of the plastic energy barrier is [4,64]

$$U_{pl} \sim \varepsilon\varepsilon_0 a_0 \propto (T_c - T)/B^{\alpha}. \tag{4}$$

Here ε_0 is the vortex line tension, and $\varepsilon = \sqrt{m_{ab}/m_c}$ is the electronic mass anisotropy (for m_{ab} and m_c are the masses in the ab plane and along the c axis, respectively). Hence, we now look at the temperature and field dependence of the plastic energy barrier $U_{pl}(H, T)$, presented in Fig. 7.

Figure 7 shows that the plastic activation energy U_{pl} in regime 2 decreases with magnetic field, consistent with plastic dynamics, as opposed to collective creep in which U_{el} increases with magnetic field [6]. Specifically, we find that $U_{pl} \propto (T_c - T)/B$ for the overdoped crystal. Notice that the data collected at different temperatures all collapse onto a single curve and appear roughly linear in the figure.

Plastic creep theory predicts $\alpha \sim 1/2$ [65,66], based on plastic deformations in crystalline solids [5]. Faster than $1/\sqrt{B}$ behavior has been previously observed [6,67–70] and associated with entangled vortex liquid behavior from *stronger* pinning due to point disorder [71] than for $\alpha \sim 1/2$. The energy U_{pl} decreases faster with increasing field because the entangled vortices become cut and disconnected [64,71], therefore moving faster (faster S).

Plotting U_{pl} versus $(T_c - T)/B$ for plastic regimes 1 and 2 on the same plot, shown in the inset to Fig. 7(a), we see that all data collapse onto the same curve. It is evident that U_{pl} rises far more rapidly with increasing $(T_c - T)/B$ than in regime 2, as plastic regime 1 includes lower fields than regime 2. Data

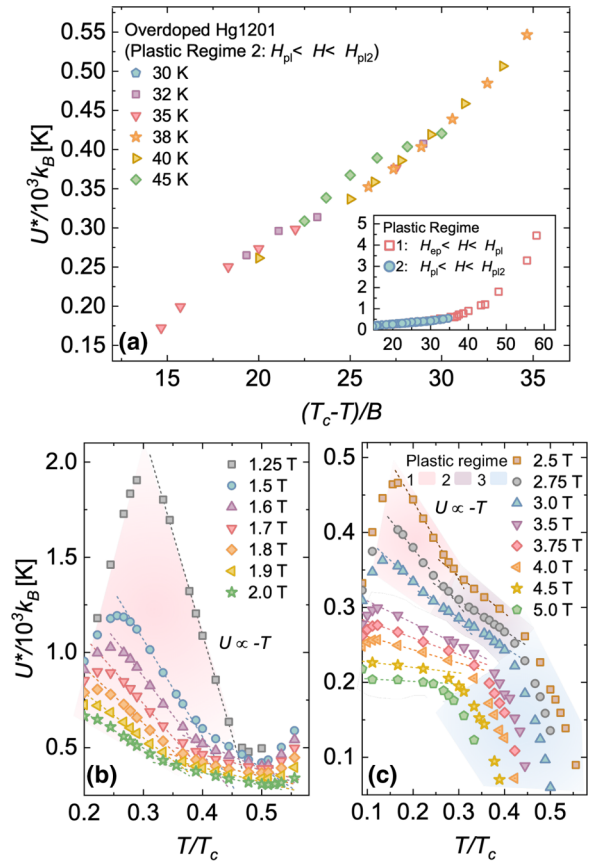

FIG. 7. (a) Energy scale U^* vs $(T_c - T)/B$ for overdoped Hg1201 sample showing that data collapses onto a single curve such that $U^* \sim 1/B$ in plastic regime 2. Inset shows collapse onto single curve for regimes 1 and 2. (a, b) U^* vs temperature, normalized to T_c, at (b) low fields and (c) higher fields. Plastic flow regimes 1, 2, and 3 identified by red, yellow, and blue shading, respectively. It is unclear whether the behavior in the unshaded region in (c) captures dynamics similar to regimes 1 or 2. Dashed lines are linear fits.

for the plastic activation barrier for regime 3 (not shown in the inset) deviates from this trend.

Equation (4) indicates that, at fixed magnetic fields, the plastic activation barrier should decrease linearly with temperature [64]. This behavior is evident in multiple regions of the $U(T/T_c)$ plot in Figs. 7(b) and 7(c), disregarding the low-field high-$T/T_c > 0.5$ data that corresponds to the anomalous peak in $S(T)$. Also, note that at high fields $\mu_0 H \gtrsim 3.5$ T and low temperatures $T/T_c < 0.3$, U_{pl} becomes relatively insensitive to temperature.

We now evaluate the possibility of a 3D-to-2D dimensional crossover causing the kinks in the plastic flow region. In highly anisotropic cuprate superconductors, the vortex lattice is composed of pancake vortices that form within the CuO_2 layers and interact both magnetically and through Josephson coupling between the layers. In the 3D regime, significant interlayer coupling causes vortices to behave as chains, somewhat aligned along the c axis, experiencing 3D-like fluctuations, resembling lines in isotropic superconductors. A couple mechanisms may induce quasi-2D behavior in which the pancakes move independently within the plane.

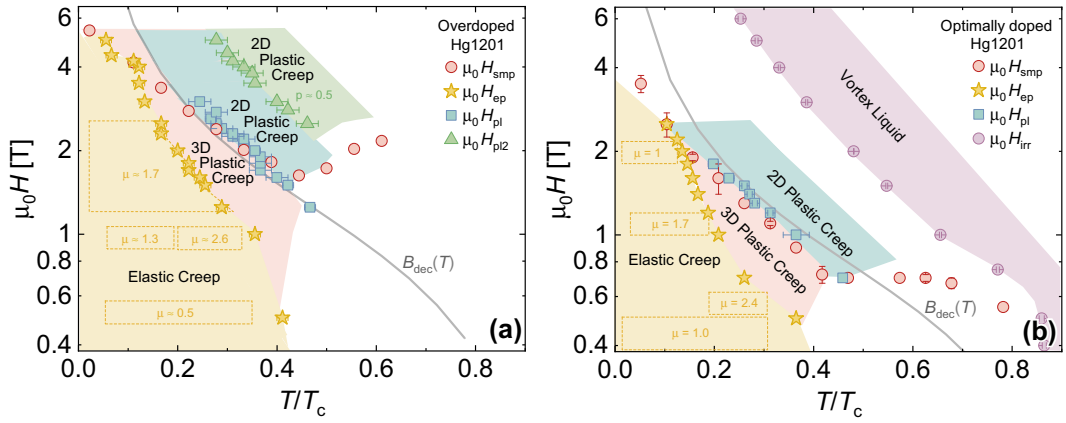

FIG. 8. Vortex phase diagram determined from creep measurements overlaid with position of second magnetization peak at $H_{\rm smp}$ for (a) overdoped and (b) optimally doped Hg1201 crystals. The gray curve is the prediction for the 3D-to-2D decoupling field based on Eq. (5). Overlap with $B_{\rm dec}$ suggests that the second magnetization peak originates from a 3D-to-2D dimensional crossover from 3D-to-2D plastic dynamics.

The strength of interactions between pancake vortices within a layer may surpass that of coupling between adjacent layers [72] or destruction of phase coherence by fluctuations may ultimately lead to Josephson decoupling [73]. Changing the magnetic field can induce this transition partially because an increase in the magnetic field reduces the intralayer vortex separation whereas the distance between planes remains fixed. A 3D-to-2D transition may manifest as a sudden change in magnetization data. When vortices become decoupled between the layers, pancake vortices within a layer can more freely reposition themselves to minimize their energy, fully exploiting available pinning centers, resulting in an increase in J_c (or slower decrease with field) [74].

Let us now consider the expected decoupling field $B_{\rm dec}(T)$ based on Josephson decoupling arising from destruction of phase coherence [75]:

$$B_{\rm dec} = \Phi_0^3[\ln(\lambda_{ab}/s) + 1.12]/4\pi\mu_0\lambda_{ab}^3\gamma^2 k_B T, \qquad (5)$$

which considers the Lawrence-Doniach expression for line tension [76]. To calculate $B_{\rm dec}(T)$ in our overdoped crystal, we know that the distance between CuO_2 planes $s = 0.952$ nm [77], $\gamma = 25$ [78], and $\lambda_{ab}(0) = 156$ nm [78]. In the case of the optimally doped crystal, we use $\lambda_{ab}(0) = 154$ nm, $\gamma = 32$ [32], and $s = 0.953$ nm [77]. For the temperature dependence of the penetration depth, we apply the two-fluid expression $\lambda_{ab}(T) = \lambda_{ab}(0)[1 - (T/T_c)^4]^{-1/2}$, which was found to accurately describe $\lambda_{ab}(T)$ in Hg1201 [78]. Based on these parameters, we plot the calculated $B_{\rm dec}(T)$ in the phase diagram in Fig. 8. Remarkably, we find striking overlap between the predicted $B_{\rm dec}(T)$, $H_{pl}(T)$, and $H_{\rm smp}(T)$ for both samples. This suggests that the second magnetization peak and crossovers in the plastic flow regime at H_{pl} originate from a dimensional crossover in the plastic flow regime. Thermal fluctuations can cause reduced instantaneous intralayer vortex separation. This may nucleate a decoupling transition to 2D dynamics, such that the 3D to 2D transition occurs at lower fields with increasing temperature [54], congruous with the SMP and plastic flow transitions delineated in the phase diagram in Fig. 8.

Lastly, we seek to understand dynamics in plastic regime 3. As the field is further increased, stronger interlayer vortex-vortex interactions stiffen the lattice, weakening vortex-defect interactions engendering a more rapid decrease in J_c [54]. In plastic regime 3, we extract a plastic exponent $|p| \sim 0.4 - 0.5$ [slope of $\log U^* - \log(1/J)$] from the data in Fig. 5(b) that is similar at all fields and consistent with the expectation of dislocation-mediated motion of vortices [6], though it is unclear what the exponent should be for 2D plastic creep.

In this work we show evidence of a dimensional crossover in the plastic flow regime. Yet there remains transitions that we have identified to regimes in which the dynamics arrangements are unclear. Further work is warranted, with a particular interest in neutron scattering studies, which could help reveal these phases and clarify the mechanism behind the unexplained transitions. For example, such studies would help evaluate whether the vortex lattice may undergo a structural transition. These results may also shed light on understanding plasticity in other systems, including materials containing skyrmions [79–81], domain walls [82,83], and charge density waves [84,85].

III. METHODS

A. Growth and structural characterization

Our study includes results from two $HgBa_2CuO_{4+x}$ (Hg1201) single crystals: an optimally doped crystal of dimensions $1.28 \times 0.84 \times 0.24$ mm^3 and an overdoped crystal of dimensions $1.5(5) \times 1.05(5) \times 0.23$ mm^3. The thickness of the overdoped sample was found by calculating the superconducting volume $V = -4\pi(1 - D)\frac{dm}{dH}$ from a measurement of the Meissner slope $\frac{dm}{dH}$, using the demagnetization factor [86] $D = 0.65$, and dividing by the measured lateral dimensions. The anisotropy γ of the samples is 32 (optimally doped [32]) and 25 (overdoped [78]).

Both samples were grown at Los Alamos National Laboratory using an encapsulated self-flux method described in Ref. [87]. The optimally doped crystal was subsequently heat-treated at 350 °C in air and quenched to room temperature

[88], whereas the overdoped crystal was heat-treated in approximately 2 bar O_2 at 300 °C. The high quality of the synthesized crystals is evidenced by the observation of large quantum oscillations in other samples of ours grown using the same method [42], which has become a standard method of growing high-quality Hg1201 crystals [32,42,43,45,89–98]. The sharpness of the superconducting transition in Fig. 2 evidences good homogeneity because the T_c is highly sensitive to doping. (Poor homogeneity would result in a broad superconducting transition.) Through magnetization, susceptibility, and electrical transport measurements, Chan has studied superconducting transitions in numerous $HgBa_2CuO_{4+\delta}$ crystals that were fabricated using this technique, cf. Refs. [42] and [94] (studied 34 crystals).

B. Magnetometry

Magnetization measurements $M(T, H, t)$ were performed using a Quantum Design (QD) SQUID magnetometer, in which the magnetic field was aligned with the sample's c axis ($H \parallel c$). The data for the overdoped crystal was collected using a QD MPMS3 system, whereas the optimally doped crystal was measured using a QD MPMS XL. This difference accounts for the lower point densities for the latter due to significantly slower measurements (slower field sweep rate).

When collecting magnetization loops $M(H)$, the field was first swept to -3 T or -4 T to establish the critical state (full flux penetration throughout the sample). The lower branch of the loop was subsequently measured as the field was ramped from 0 to 7 T, and the upper branch was collected as the field was swept down to -7 T, then ramped back up to zero.

Creep data were taken using the standard approach [49]. First, we establish the critical state sweeping the field high enough that vortices, which first enter at the sample peripheries, permeate the center of the sample and the Bean critical state model defines the vortex distribution. Following standard practice, this requires a sweep of $\Delta H > 4H^\star$ (for $H^\star$ is the field of full flux penetration) and verification that the initial $M(T, H)$ lies on the magnetization loop. Subsequently, we capture the decay in the magnetization $M(t)$ by repeatedly measuring M every $\sim$10 s at a fixed T and H: we measure $m(t)$ for an hour in the upper branch, preceded by a brief measurement in the lower branch that enables determining the background (e.g., from sample holders). After subtracting this background (average of the upper and lower branches) and adjusting the time to account for the difference between the initial application of the magnetic field and the first measurement, $S \equiv d \ln m / d \ln t$ was determined from the slope of a linear fit to $\ln m$ versus $\ln t$.

All data presented in this work are available from the corresponding authors upon reasonable request.

ACKNOWLEDGMENTS

We would like to thank V. Vinokur, C. J. O. Reichhardt, and C. Reichhardt for useful discussions regarding the plastic flow regime. This material is based upon work supported by the National Science Foundation under Grant No. DMR-1905909 (magnetization measurements, data analysis, and manuscript composition). M.K.C. acknowledges support from the U.S. Department of Energy, "Science at 100 T" (crystal synthesis). E.D.B. acknowledges support from the U.S. Department of Energy (DOE), Office of Basic Energy Sciences, Division of Materials Science and Engineering, under the Quantum Fluctuations in Narrow-Band Systems.

S.E. conceived and designed the experiment. S.E. and H.M.C. collected and analyzed the magnetization data. M.B.V. wrote software to perform data analysis. M.K.C. and E.D.B. grew the samples. B.G. performed transmission electron microscopy and analyzed the microstructural data. S.E. wrote the manuscript. All authors commented on the manuscript.

[1] G. Grüner, The dynamics of charge-density waves, Rev. Mod. Phys. **60**, 1129 (1988).

[2] Y. Nii, A. Kikkawa, Y. Taguchi, Y. Tokura, and Y. Iwasa, Elastic Stiffness of a Skyrmion Crystal, Phys. Rev. Lett. **113**, 267203 (2014).

[3] S. Eley, A. Glatz, and R. Willa, Challenges and transformative opportunities in superconductor vortex physics, J. Appl. Phys. **130**, 050901 (2021).

[4] G. Blatter, M. V. Feigel'man, V. B. Geshkenbein, A. I. Larkin, and V. M. Vinokur, Vortices in high-temperature superconductors, Rev. Mod. Phys. **66**, 1125 (1994).

[5] J. P. Hirth and J. Lothe, *Theory of Dislocations* (Wiley, New York, 1982).

[6] Y. Abulafia, A. Shaulov, Y. Wolfus, R. Prozorov, L. Burlachkov, Y. Yeshurun, D. Majer, E. Zeldov, H. Wühl, V. B. Geshkenbein, and V. M. Vinokur, Plastic Vortex Creep in $YBa_2Cu_3O_{7-x}$ crystals, Phys. Rev. Lett. **77**, 1596 (1996).

[7] I. Aranson and V. Vinokur, Surface Instabilities and Plastic Deformation of Vortex Lattices, Phys. Rev. Lett. **77**, 3208 (1996).

[8] D. W. Braun, G. W. Crabtree, H. G. Kaper, A. E. Koshelev, G. K. Leaf, D. M. Levine, and V. M. Vinokur, Structure of a Moving Vortex Lattice, Phys. Rev. Lett. **76**, 831 (1996).

[9] H. J. Jensen, Y. Brechet, and A. Brass, On the threshold pinning force in type II superconducting films, J. Low Temp. Phys. **74**, 293 (1989).

[10] A. E. Koshelev and V. M. Vinokur, Dynamic Melting of the Vortex Lattice, Phys. Rev. Lett. **73**, 3580 (1994).

[11] H. J. Jensen, A. Brass, A. C. Shi, and A. J. Berlinsky, Simulations of the onset of diffusion in a flux-line lattice in a random potential, Phys. Rev. B **41**, 6394 (1990).

[12] M. V. Feigel'man, V. B. Geshkenbein, A. I. Larkin, and V. M. Vinokur, Theory of Collective Flux Creep, Phys. Rev. Lett. **63**, 2303 (1989).

[13] S. S. Banerjee, S. Ramakrishnan, A. K. Grover, G. Ravikumar, P. K. Mishra, V. C. Sahni, C. V. Tomy, G. Balakrishnan, D. M. Paul, P. L. Gammel, D. J. Bishop, E. Bucher, M. J. Higgins, and S. Bhattacharya, Peak effect, plateau effect, and fishtail anomaly: The reentrant amorphization of vortex matter in $2H-NbSe_2$, Phys. Rev. B **62**, 11838 (2000).

[14] F. Zuo, S. Khizroev, X. Jiang, J. L. Peng, and R. L. Greene, Surface barriers and two-dimensional-collective pinning in single crystal $Nd_{1.85}Ce_{0.15}CuO_{4-\delta}$ superconductors, J. Appl. Phys. **76**, 6953 (1994).

[15] D. Miu, T. Noji, T. Adachi, Y. Koike, and L. Miu, On the nature of the second magnetization peak in $FeSe_{1-x}Te_x$ single crystals, Supercond. Sci. Technol. **25**, 115009 (2012).

[16] L. Fang, Y. Jia, J. A. Schlueter, A. Kayani, Z. L. Xiao, H. Claus, U. Welp, A. E. Koshelev, G. W. Crabtree, and W.-K. Kwok, Doping- and irradiation-controlled pinning of vortices in $BaFe_2(As_{1-x}p_x)_2$ single crystals, Phys. Rev. B **84**, 140504(R) (2011).

[17] W. Zhou, X. Xing, W. Wu, H. Zhao, and Z. Shi, Second magnetization peak effect, vortex dynamics, and flux pinning in 112-type superconductor $Ca_{0.8}La_{0.2}Fe_{1-x}Co_xAs_2$, Sci. Rep. **6**, 22278 (2016).

[18] S. Salem-Sugui, L. Ghivelder, A. D. Alvarenga, L. F. Cohen, K. A. Yates, K. Morrison, J. L. Pimentel, H. Luo, Z. Wang, and H.-H. Wen, Flux dynamics associated with the second magnetization peak in the iron pnictide $Ba_{1-x}K_xFe_2As_2$, Phys. Rev. B **82**, 054513 (2010).

[19] A. K. Pramanik, L. Harnagea, C. Nacke, A. U. B. Wolter, S. Wurmehl, V. Kataev, and B. Büchner, Fishtail effect and vortex dynamics in LiFeAs single crystals, Phys. Rev. B **83**, 094502 (2011).

[20] B. Shen, P. Cheng, Z. Wang, L. Fang, C. Ren, L. Shan, and H. H. Wen, Flux dynamics and vortex phase diagram in $Ba(Fe_{1-x}Co_x)_2As_2$ single crystals revealed by magnetization and its relaxation, Phys. Rev. B **81**, 014503 (2010).

[21] A. M. Ionescu, D. Miu, A. Crisan, and L. Miu, Pinning-induced vortex-system disordering at the origin of the second magnetization peak in superconducting single crystals, J. Supercond. Novel Magn. **31**, 2329 (2018).

[22] R. Prozorov, N. Ni, M. A. Tanatar, V. G. Kogan, R. T. Gordon, C. Martin, E. C. Blomberg, P. Prommapan, J. Q. Yan, S. L. Bud'ko, and P. C. Canfield, Vortex phase diagram of $Ba(Fe_{0.93}Co_{0.07})_2As_2$ single crystals, Phys. Rev. B **78**, 224506 (2008).

[23] M. Bonura, E. Giannini, R. Viennois, and C. Senatore, Temperature and time scaling of the peak-effect vortex configuration in $FeTe_{0.7}Se_{0.3}$, Phys. Rev. B **85**, 134532 (2012).

[24] Y. Nakajima, Y. Tsuchiya, T. Taen, T. Tamegai, S. Okayasu, and M. Sasase, Enhancement of critical current density in Co-doped $BaFe_2As_2$ with columnar defects introduced by heavy-ion irradiation, Phys. Rev. B **80**, 012510 (2009).

[25] M. Polichetti, A. Galluzzi, K. Buchkov, V. Tomov, E. Nazarova, A. Leo, G. Grimaldi, and S. Pace, A precursor mechanism triggering the second magnetization peak phenomenon in superconducting materials, Sci. Rep. **11**, 7247 (2021).

[26] P. Chowdhury, H.-J. Kim, I.-S. Jo, and S.-I. Lee, Peak anomaly and irreversible magnetization in $Tl_2Ba_2CaCu_2O_8$ single crystals, Physica C **384**, 411 (2003).

[27] M. Konczykowski, S. Colson, C. J. van der Beek, M. V. Indenbom, P. Kes, and E. Zeldov, Magnetic relaxation in the vicinity of second magnetization peak in BSCCO crystals, Physica C **332**, 219 (2000).

[28] M. Boudissa, R. Halimi, K. Frikach, and S. Senoussi, Fishtail effect in twinned and detwinned YBCO single crystals, Phys. Status Solidi C **3**, 3044 (2006).

[29] L. Miu, E. Cimpoiasu, T. Stein, and C. Almasan, Plastic vortex creep above the second magnetization peak in $Bi_2Sr_2CaCu_2O_{8+\delta}$ single crystals, Physica C **334**, 1 (2000).

[30] H. Küpfer, S. N. Gordeev, W. Jahn, R. Kresse, R. Meier-Hirmer, T. Wolf, A. A. Zhukov, K. Salama, and D. Lee, Phase diagram of flux creep in melt-textured and single-crystalline $YBa_2Cu_3O_{7-\delta}$, Phys. Rev. B **50**, 7016 (1994).

[31] K. Katayama, Y. Yoshida, S. Kawamata, T. Ishida, K. Shibata, T. Sasaki, N. Kobayashi, S. Adachi, and S. Tajima, Peak effect and vortex phase diagram of $YBa_2Cu_4O_8$, Physica C **392-396**, 382 (2003).

[32] S. Eley, R. Willa, M. K. Chan, E. D. Bauer, and L. Civale, Vortex phases and glassy dynamics in the highly anisotropic superconductor $HgBa_2CuO_{4+\delta}$, Sci. Rep. **10**, 10239 (2020).

[33] A. Daignere, T. Aouaroun, and C. Simon, Absence of dynamical crossover in the vortex creep near by the second peak effect in superconducting Hg-1201 single crystals, Eur. Phys. J. B **16**, 397 (2000).

[34] G. Villard, A. Daignere, D. Pelloquin, and A. Maignan, Effect of underdoping on the superconductivity of $(Hg,Cu)Ba_2CuO_4$, Physica C **314**, 196 (1999).

[35] M. Pissas, D. Stamopoulos, E. Moraitakis, G. Kallias, D. Niarchos, and M. Charalambous, Magnetic relaxation measurements in the region of the second magnetization peak in a $HgBa_2CuO_{4+\delta}$ single crystal, Phys. Rev. B **59**, 12121 (1999).

[36] M. Pissas, E. Moraitakis, G. Kallias, A. Terzis, D. Niarchos, and M. Charalambous, Irreversibility line in superconducting $HgBa_2CuO_{4+\delta}$ single crystals, Phys. Rev. B **58**, 9536 (1998).

[37] D. Stamopoulos and M. Pissas, Hysteretic behavior of the vortex lattice at the onset of the second peak for the $HgBa_2CuO_{4+\delta}$, Phys. Rev. B **65**, 134524 (2002).

[38] R. Gilardi, J. Mesot, A. Drew, U. Divakar, S. L. Lee, E. M. Forgan, O. Zaharko, K. Conder, V. K. Aswal, C. D. Dewhurst, R. Cubitt, N. Momono, and M. Oda, Direct Evidence for an Intrinsic Square Vortex Lattice in the Overdoped High-T_c Superconductor $La_{1.83}Sr_{0.17}CuO_{4+d}$, Phys. Rev. Lett. **88**, 217003 (2002).

[39] B. Rosenstein, B. Y. Shapiro, I. Shapiro, Y. Bruckental, A. Shaulov, and Y. Yeshurun, Peak effect and square-to-rhombic vortex lattice transition in $La_{2-x}Sr_xCuO_4$, Phys. Rev. B **72**, 144512 (2005).

[40] R. Kopeliansky, A. Shaulov, B. Y. Shapiro, Y. Yeshurun, B. Rosenstein, J. J. Tu, L. J. Li, G. H. Cao, and Z. A. Xu, Possibility of vortex lattice structural phase transition in the superconducting pnictide $Ba(Fe_{0.925}Co_{0.075})_2As_2$, Phys. Rev. B **81**, 092504 (2010).

[41] L. Miu, A. M. Ionescu, D. Miu, M. Burdusel, P. Badica, D. Batalu, and A. Crisan, Second magnetization peak, rhombic-to-square Bragg vortex glass transition, and intersecting magnetic hysteresis curves in overdoped $BaFe_2(As_{1-x}P_x)_2$ single crystals, Sci. Rep. **10**, 17274 (2020).

[42] M. K. Chan, R. D. McDonald, B. J. Ramshaw, J. B. Betts, A. Shekhter, E. D. Bauer, and N. Harrison, Extent of Fermi-surface reconstruction in the high-temperature superconductor $HgBa_2CuO_{4+\delta}$, Proc. Natl. Acad. Sci. USA **117**, 9782 (2020).

[43] N. Barišić, S. Badoux, M. K. Chan, C. Dorow, W. Tabis, B. Vignolle, G. Yu, J. Béard, X. Zhao, C. Proust, and M. Greven, Universal quantum oscillations in the underdoped cuprate superconductors, Nat. Phys. **9**, 761 (2013).

[44] W. Tabis, Y. Li, M. L. Tacon, L. Braicovich, A. Kreyssig, M. Minola, G. Dellea, E. Weschke, M. J. Veit, M. Ramazanoglu, A. I. Goldman, T. Schmitt, G. Ghiringhelli, N. Barišić, M. K. Chan, C. J. Dorow, G. Yu, X. Zhao, B. Keimer, and M. Greven, Charge order and its connection with Fermi-liquid charge transport in a pristine high-T_c cuprate, Nat. Commun. **5**, 5875 (2014).

[45] N. Barišić, Y. Li, X. Zhao, Y.-C. Cho, G. Chabot-Couture, G. Yu, and M. Greven, Demonstrating the model nature of the high-temperature superconductor $HgBa_2CuO_{4+\delta}$, Phys. Rev. B **78**, 054518 (2008).

[46] D. Pelloquin, V. Hardy, A. Maignan, and B. Raveau, Single crystals of the 96 K superconductor (Hg,Cu)$Ba_2CuO_{4+\delta}$ growth, structure and magnetism, Physica C **273**, 205 (1997).

[47] J. Wagner, P. Radaelli, D. Hinks, J. Jorgensen, J. Mitchell, B. Dabrowski, G. Knapp, and M. Beno, Structure and superconductivity of $HgBa_2CuO_{4+\delta}$, Physica C **210**, 447 (1993).

[48] V. Viallet, A. Bertinotti, J.-F. Marucco, D. Colson, L. Fruchter, G. L. Bras, V. Vulcanescu, and J. Hammann, Superconductivity, X-ray structure and non stoichiometry of $HgBa_2Cu_{4+\delta}$, Physica C **282-287**, 1073 (1997).

[49] Y. Yeshurun, A. P. Malozemoff, and A. Shaulov, Magnetic relaxation in high-temperature superconductors, Rev. Mod. Phys. **68**, 911 (1996).

[50] V. Vinokur, P. Kes, and A. Koshelev, The 2D collective creep exponents reconsidered, Physica C **248**, 179 (1995).

[51] A. Narlikar, *HTS Thin Film and More on Vortex Studies*, Studies of High Temperature Superconductors (Nova Science Publishers, Hauppauge, NY, 2005).

[52] See Supplemental Material at http://link.aps.org/supplemental/10.1103/PhysRevB.107.104509 for figures showing the decay in the magnetization over time.

[53] J. R. Thompson, Y. R. Sun, L. Civale, A. P. Malozemoff, M. W. McElfresh, A. D. Marwick, and F. Holtzberg, Effect of flux creep on the temperature dependence of the current density in Y-Ba-Cu-O crystals, Phys. Rev. B **47**, 14440 (1993).

[54] C. Olson, C. Reichhardt, R. T. Scalettar, G. Zimanyi, and N. Gronbech-Jensen, Disordering transitions in vortex matter: peak effect and phase diagram, Physica C **384**, 143 (2003).

[55] N. Haberkorn, M. Miura, B. Maiorov, G. F. Chen, W. Yu, and L. Civale, Strong pinning and elastic to plastic vortex crossover in Na-doped $CaFe_2As_2$ single crystals, Phys. Rev. B **84**, 094522 (2011).

[56] V. Rouco, E. Bartolomé, B. Maiorov, A. Palau, L. Civale, X. Obradors, and T. Puig, Vortex creep in TFA-YBCO nanocomposite films, Supercond. Sci. Technol. **27**, 115008 (2014).

[57] Y. Sun, T. Taen, Y. Tsuchiya, S. Pyon, Z. Shi, and T. Tamegai, Magnetic relaxation and collective vortex creep in $FeTe_{0.6}Se_{0.4}$ single crystal, Europhys. Lett. **103**, 57013 (2013).

[58] S. Sundar, S. Salem-Sugui, H. S. Amorim, H.-H. Wen, K. A. Yates, L. F. Cohen, and L. Ghivelder, Plastic pinning replaces collective pinning as the second magnetization peak disappears in the pnictide superconductor $Ba_{0.75}K_{0.25}Fe_2As_2$, Phys. Rev. B **95**, 134509 (2017).

[59] T. Taen, Y. Nakajima, T. Tamegai, and H. Kitamura, Enhancement of critical current density and vortex activation energy in proton-irradiated Co-doped $BaFe_2As_2$, Phys. Rev. B **86**, 094527 (2012).

[60] Y. Sun, S. Pyon, T. Tamegai, R. Kobayashi, T. Watashige, S. Kasahara, Y. Matsuda, and T. Shibauchi, Critical current density, vortex dynamics, and phase diagram of single-crystal FeSe, Phys. Rev. B **92**, 144509 (2015).

[61] A. Galluzzi, M. Polichetti, K. Buchkov, E. Nazarova, D. Mancusi, and S. Pace, Critical current and flux dynamics in Ag-doped FeSe superconductor, Supercond. Sci. Technol. **30**, 025013 (2017).

[62] A. E. Tahan, G. Jakob, D. Miu, I. Ivan, P. Badica, and L. Miu, Vortex creep crossover in YBCO/PrBCO superlattices during standard magnetization relaxation measurements, Supercond. Sci. Technol. **24**, 045014 (2011).

[63] L. Miu, M. Basset, G. Jakob, H. Rodriguez, and H. Adrian, Nondiverging vortex pinning barriers at low current densities across the putative elastic vortex-glass–vortex-liquid transition in $YBa_2Cu_3O_{7-\delta}$ films, Phys. Rev. B **64**, 220502(R) (2001).

[64] V. M. Vinokur, M. V. Feigel'man, V. B. Geshkenbein, and A. I. Larkin, Resistivity of High-T_c Superconductors in a Vortex-Liquid State, Phys. Rev. Lett. **65**, 259 (1990).

[65] J. Kierfeld, H. Nordborg, and V. M. Vinokur, Theory of Plastic Vortex Creep, Phys. Rev. Lett. **85**, 4948 (2000).

[66] V. Geshkenbein, A. Larkin, M. F. Man, and V. Vinokur, Flux pinning and creep in high-T_c superconductors, Physica C **162-164**, 239 (1989).

[67] W. J. Choi, Y. I. Seo, D. Ahmad, and Y. S. Kwon, Thermal activation energy of 3D vortex matter in $NaFe_{1-x}Co_xAs$ ($x = 0.01$, 0.03 and 0.07) single crystals, Sci. Rep. **7**, 10900 (2017).

[68] Z. Wu, J. Tao, X. Xu, L. Qiu, S. Yang, and Z. Wang, Anisotropic flux pinning energy in $FeSe_xTe_{1-x}$ single crystals, Physica C **528**, 39 (2016).

[69] A. Wang and C. Petrovic, Vortex pinning and irreversibility fields in $FeS_{1x}Se_x$ ($x = 0$, 0.06), Appl. Phys. Lett. **110**, 232601 (2017).

[70] M. A. Obolenskii, A. V. Bondarenko, A. A. Prodan, R. V. Vovk, M. G. Revyakina, M. Pissas, G. Kallias, D. Niarchos, and T. R. Arouri, Vortex dynamics in YBCO single crystals at high temperatures, in *Magnetic and Superconducting Materials* (World Scientific Publishing Company, Singapore, 2000), pp. 447–460.

[71] D. López, L. Krusin-Elbaum, H. Safar, E. Righi, F. de la Cruz, S. Grigera, C. Feild, W. K. Kwok, L. Paulius, and G. W. Crabtree, Pinned Vortex Liquid above the Critical Point of the First-Order Melting Transition: A Consequence of Pointlike Disorder, Phys. Rev. Lett. **80**, 1070 (1998).

[72] V. Vinokur, P. Kes, and A. Koshelev, Flux pinning and creep in very anisotropic high temperature superconductors, Physica C **168**, 29 (1990).

[73] G. Deutscher and A. Kapitulnik, Breakdown field in highly anisotropic superconductors, Physica A **168**, 338 (1990).

[74] A. K. Pradhan, S. B. Roy, P. Chaddah, C. Chen, and B. M. Wanklyn, Magnetic properties of single-crystal $Bi_2Sr_2CaCu_2O_8$: Experimental evidence for a dimensional crossover, Phys. Rev. B **49**, 12984 (1994).

[75] V. Hardy, A. Wahl, A. Ruyter, A. Maignan, C. Martin, L. Coudrier, J. Provost, and C. Simon, The fishtail effect in different T1 based single crystals: A possible interplay with the electronic anisotropy, Physica C **232**, 347 (1994).

[76] J. R. Clem, Fundamentals of vortices in the high-temperature superconductors, Supercond. Sci. Technol. **5**, S33 (1992).

[77] A. M. Balagurov, D. V. Sheptyakov, V. L. Aksenov, E. V. Antipov, S. N. Putilin, P. G. Radaelli, and M. Marezio, Structure

of $HgBa_2CuO_{4+\delta}(0.06 < \delta < 0.19)$ at ambient and high pressure, Phys. Rev. B **59**, 7209 (1999).

[78] J. Hofer, J. Karpinski, M. Willemin, G. Meijer, E. Kopnin, R. Molinski, H. Schwer, C. Rossel, and H. Keller, Doping dependence of superconducting parameters in $HgBa_2CuO_{4+\delta}$ single crystals, Physica C **297**, 103 (1998).

[79] C. Olson Reichhardt, S. Lin, D. Ray, and C. Reichhardt, Comparing the dynamics of skyrmions and superconducting vortices, Physica C **503**, 52 (2014).

[80] C. Reichhardt and C. J. O. Reichhardt, Depinning and nonequilibrium dynamic phases of particle assemblies driven over random and ordered substrates: A review, Rep. Prog. Phys. **80**, 026501 (2017).

[81] C. Reichhardt, D. Ray, and C. J. O. Reichhardt, Collective Transport Properties of Driven Skyrmions with Random Disorder, Phys. Rev. Lett. **114**, 217202 (2015).

[82] S. Lemerle, J. Ferré, C. Chappert, V. Mathet, T. Giamarchi, and P. Le Doussal, Domain Wall Creep in an Ising Ultrathin Magnetic Film, Phys. Rev. Lett. **80**, 849 (1998).

[83] A. K. Lindquist, J. M. Feinberg, R. J. Harrison, J. C. Loudon, and A. J. Newell, Domain wall pinning and dislocations: Investigating magnetite deformed under conditions analogous to nature using transmission electron microscopy, J. Geophys. Res. Solid Earth **120**, 1415 (2015).

[84] A. F. Isakovic, P. G. Evans, J. Kmetko, K. Cicak, Z. Cai, B. Lai, and R. E. Thorne, Shear Modulus and Plasticity of a Driven Charge Density Wave, Phys. Rev. Lett. **96**, 046401 (2006).

[85] S. Brazovskii and T. Nattermann, Pinning and sliding of driven elastic systems: From domain walls to charge density waves, Adv. Phys. **53**, 177 (2004).

[86] E. Pardo, D. X. Chen, and A. Sanchez, Demagnetizing factors for completely shielded rectangular prisms, J. Appl. Phys. **96**, 5365 (2004).

[87] X. Zhao, G. Yu, Y.-C. Cho, G. Chabot-Couture, N. Barišić, P. Bourges, N. Kaneko, Y. Li, L. Lu, E. M. Motoyama, O. P. Vajk, and M. Greven, Crystal growth and characterization of the model high-temperature superconductor $HgBa_2CuO_{4+\delta}$, Adv. Mater. **18**, 3243 (2006).

[88] A. Yamamoto, W.-Z. Hu, and S. Tajima, Thermoelectric power and resistivity of $HgBa_2CuO_{4+\delta}$ over a wide doping range, Phys. Rev. B **63**, 024504 (2000).

[89] D. D. Xia, G. Yu, X. Zhao, B. Li, X. Liu, L. Ji, M. K. Chan, and M. Greven, Temperature and field dependence of the anisotropy parameter for the high-temperature superconductor $HgBa_2CuO_{4+\delta}$, Supercond. Sci. Technol. **25**, 115010 (2012).

[90] A. M. Mounce, S. Oh, J. A. Lee, W. P. Halperin, A. P. Reyes, P. L. Kuhns, M. K. Chan, C. Dorow, L. Ji, D. Xia, X. Zhao, and M. Greven, Absence of Static Loop-Current Magnetism at the Apical Oxygen Site in $HgBa_2CuO_{4+\delta}$ from NMR, Phys. Rev. Lett. **111**, 187003 (2013).

[91] Y. Li, M. Le Tacon, Y. Matiks, A. V. Boris, T. Loew, C. T. Lin, L. Chen, M. K. Chan, C. Dorow, L. Ji, N. Barišić, X. Zhao, M. Greven, and B. Keimer, Doping-Dependent Photon Scattering Resonance in the Model High-Temperature Superconductor $HgBa_2CuO_{4+\delta}$ Revealed by Raman Scattering and Optical Ellipsometry, Phys. Rev. Lett. **111**, 187001 (2013).

[92] I. M. Vishik, N. Barišić, M. K. Chan, Y. Li, D. D. Xia, G. Yu, X. Zhao, W. S. Lee, W. Meevasana, T. P. Devereaux, M. Greven, and Z.-X. Shen, Angle-resolved photoemission spectroscopy study of $Hgba_2Cuo_{4+\delta}$, Phys. Rev. B **89**, 195141 (2014).

[93] D. Rybicki, J. Kohlrautz, J. Haase, M. Greven, X. Zhao, M. K. Chan, C. J. Dorow, and M. J. Veit, Electronic spin susceptibilities and superconductivity in $HgBa_2CuO_{4+\delta}$ from nuclear magnetic resonance, Phys. Rev. B **92**, 081115(R) (2015).

[94] M. K. Chan, C. J. Dorow, L. Mangin-Thro, Y. Tang, Y. Ge, M. J. Veit, G. Yu, X. Zhao, A. D. Christianson, J. T. Park, Y. Sidis, P. Steffens, D. L. Abernathy, P. Bourges, and M. Greven, Commensurate antiferromagnetic excitations as a signature of the pseudogap in the tetragonal high-T_c cuprate $HgBa_2CuO_{4+\delta}$, Nat. Commun. **7**, 10819 (2016).

[95] M. K. Chan, Y. Tang, C. J. Dorow, J. Jeong, L. Mangin-Thro, M. J. Veit, Y. Ge, D. L. Abernathy, Y. Sidis, P. Bourges, and M. Greven, Hourglass Dispersion and Resonance of Magnetic Excitations in the Superconducting State of the Single-Layer Cuprate $HgBa_2CuO_{4+\delta}$ near Optimal Doping, Phys. Rev. Lett. **117**, 277002 (2016).

[96] J. A. Lee, Y. Xin, W. P. Halperin, A. P. Reyes, P. L. Kuhns, and M. K. Chan, Coherent charge and spin density waves in underdoped $HgBa_2CuO_{4+\delta}$, New J. Phys. **19**, 033024 (2017).

[97] Y. Tang, L. Mangin-Thro, A. Wildes, M. K. Chan, C. J. Dorow, J. Jeong, Y. Sidis, M. Greven, and P. Bourges, Orientation of the intra-unit-cell magnetic moment in the high-T_c superconductor $HgBa_2Cuo_{4+\delta}$, Phys. Rev. B **98**, 214418 (2018).

[98] L. Wang, G. He, Z. Yang, M. Garcia-Fernandez, A. Nag, K. Zhou, M. Minola, M. L. Tacon, B. Keimer, Y. Peng, and Y. Li, Paramagnons and high-temperature superconductivity in a model family of cuprates, Nat. Commun. **13**, 3163 (2022).